


Review

# Recent Developments in 3D Printing of Rare-Earth-Free Permanent Magnets

Chitnarong Sirisathitkul<sup>1,2,3</sup> and Yaowarat Sirisathitkul<sup>1,4,\*</sup> 

<sup>1</sup> Functional Materials and Nanotechnology Center of Excellence, Walailak University, Nakhon Si Thammarat 80160, Thailand

<sup>2</sup> Thailand Center of Excellence in Physics, Ministry of Higher Education, Science, Research and Innovation, Bangkok 10400, Thailand

<sup>3</sup> Division of Physics, School of Science, Walailak University, Nakhon Si Thammarat 80160, Thailand

<sup>4</sup> School of Engineering and Technology, Walailak University, Nakhon Si Thammarat 80160, Thailand

\* Correspondence: syaowara@mail.wu.ac.th

**Abstract:** This article reviews the advances in additive manufacturing of magnetic ceramics and alloys without rare-earth elements. Near-net-shaped permanent magnets with varying shapes and dimensions overcome traditional limitations of the cast, sintered, and bonded magnets. The published articles are categorized based on material types and 3D printing techniques. Selective laser melting and electron beam melting were predominantly used to produce alnico magnets. In addition to the electron beam melting, manganese aluminium-based alloys were successfully printed by fuse filament fabrication. By incorporating magnetic powders in polymers and then printing via extrusion, the fuse filament fabrication was also used to produce strontium ferrite magnets. Moreover, hard ferrites were printed by stereolithography and extrusion free-forming, without drawing composites into filaments. Magnetic properties in some cases are comparable to those of conventional magnets with the same compositions. Currently, available software packages can simulate magnetic fields for designing magnets and optimize the integration in electrical machines. These developments open up opportunities for next-generation permanent magnet applications.



**Citation:** Sirisathitkul, C.;

Sirisathitkul, Y. Recent Developments in 3D Printing of Rare-Earth-Free Permanent Magnets. *Inventions* **2022**, *7*, 71. <https://doi.org/10.3390/inventions7030071>

Academic Editor: Joshua M. Pearce

Received: 22 July 2022

Accepted: 16 August 2022

Published: 22 August 2022

**Publisher's Note:** MDPI stays neutral with regard to jurisdictional claims in published maps and institutional affiliations.



**Copyright:** © 2022 by the authors. Licensee MDPI, Basel, Switzerland. This article is an open access article distributed under the terms and conditions of the Creative Commons Attribution (CC BY) license (<https://creativecommons.org/licenses/by/4.0/>).

**Keywords:** additive manufacturing; 3D printer; permanent magnet; hard ferrite; manganese-based alloy

## 1. Introduction

Large numbers of permanent magnets are used annually as essential components in electrical generators, motors, magnetrons, hard disk drives, and loudspeakers. Moreover, permanent magnets are vital to the inventions of novel wind turbines, energy harvesters, magnetic refrigerators, flywheel energy storage systems, and electric vehicles. The efficiency of these devices is improved with increasing remanence, corresponding to magnetic flux density supplied by the magnets. The other important characteristic of the magnet is its ability to withstand demagnetization, referred to as coercivity. It follows that the permanent magnet development has been emphasized on raising the remanence and the coercivity to enhance the maximum energy product [1,2]. The maximum energy product over 50 MGOe has been obtained in neodymium–iron–boron (Nd-Fe-B)-based magnets. Commercial Nd-Fe-B magnets are commonly manufactured with the addition of heavy rare-earth dysprosium (Dy). Hard ferrites provide an alternative without rare-earth elements, but their maximum energy products are lower than 10 MGOe [3]. With increasing concern over the rare-earth element supply [4], other rare-earth-free magnets are attracting more interest [5,6]. Manganese-based alloys, including manganese bismuth (MnBi), manganese gallium (MnGa), and manganese aluminium (MnAl), were investigated as ‘gap magnets’ to fill applications between those of low-cost ferrites and high-performance rare-earth magnets [7–10]. Maximum energy products of manganese-based alloys are 4–8 MGOe, but these magnets possess desirable mechanical properties and high-temperature

performance. Interestingly, the maximum energy product can also be enhanced by exploiting the interaction between hard and soft magnetic nanostructures. Novel magnets have been produced in the form of exchange-coupled nanocomposites containing hard and soft magnetic phases [5,11].

The advent of new devices and designs demands permanent magnets with diverse shapes and dimensions. However, such variations are limited by conventional processes. Traditional permanent magnets are classified into the cast, sintered, and bonded magnets. Examples of polymeric binders used in bonded magnets to improve the processability and mechanical properties are epoxies, polyamide, polyester, and polytetrafluoroethylene. In addition to compression molding (exemplified by Figure 1a), bonded magnets can be manufactured by means of extrusion, calendaring, and injection molding (exemplified by Figure 1b). For all types of commercial magnets, the requisite final machining increases the cost and material waste.

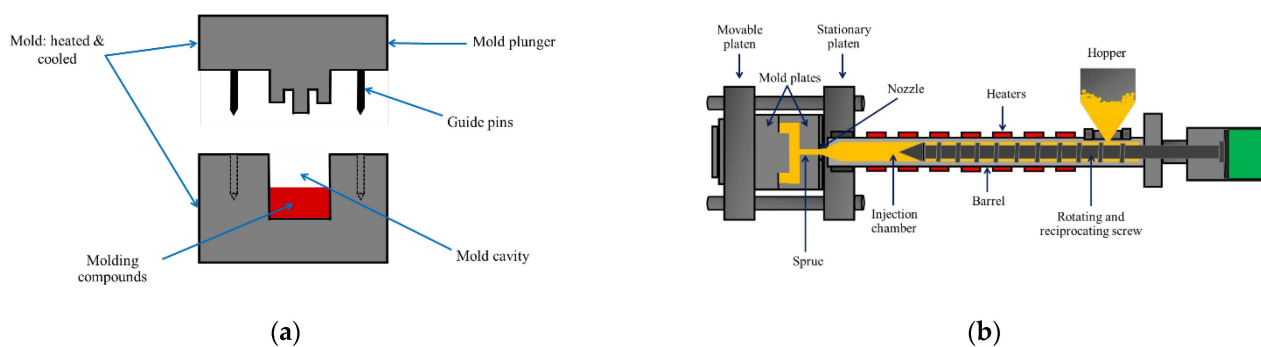


**Figure 1.** Examples of traditional manufacturing processes: (a) compression molding; (b) injection molding.

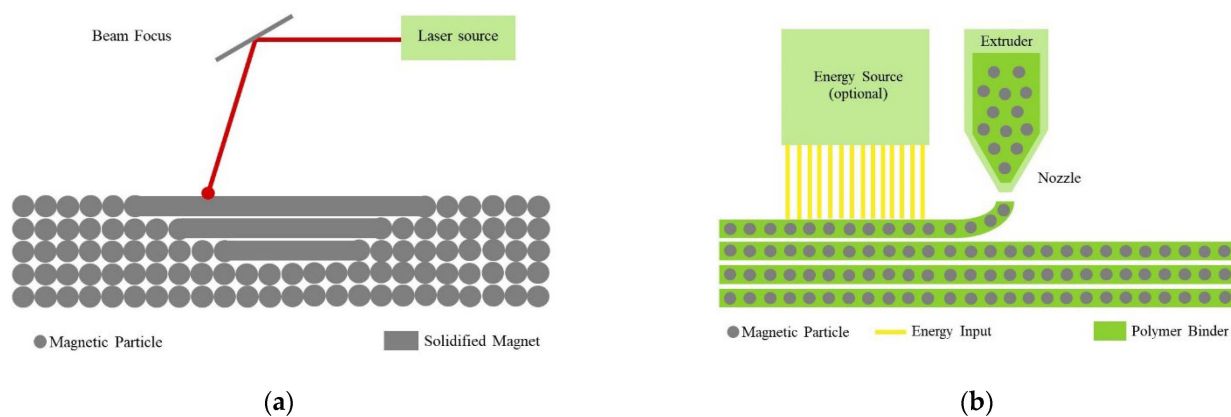
Additive manufacturing or three-dimensional (3D) printing has been developed and used in various industries over the past decade [12]. The manufacturing costs and wastes are reduced because expensive molds and extensive machining are no longer necessary. For permanent magnets, the Nd-Fe-B types were majorly investigated in earlier works owing to their higher maximum energy products. It follows that the existing reviewed articles on the development of 3D-printed magnets are focused on Nd-Fe-B [13–19]. This brief review turns attention toward 3D-printed rare-earth-free permanent magnets because their magnetic properties reported in several published articles were comparable to those obtained from conventional manufacturing. The following section summarizes the 3D printing techniques available for material development. In Sections 3 and 4, rare-earth-free permanent magnets are classified into magnetic alloys and ceramics, whose magnetic properties are related to material composition and process parameters in each 3D printing technique. The implementation and the computer software used in the design and optimization of magnets are described before the conclusion.

## 2. 3D Printing Techniques for Magnetic Materials

Numerous 3D printing technologies are classified and summarized in Table 1. Some methods have already been investigated for manufacturing hard and soft magnetic components. Stereolithography, binder jetting, selective laser melting, electron beam melting, extrusion free-forming, and fuse filament fabrication have shown significant benefits in producing near-net-shape permanent magnets with minimal final machining [13–19]. As schematically shown in Figure 2, these 3D printing techniques can fabricate complex structures that are difficult to obtain from conventional methods with minimal material waste.

**Table 1.** Classification of 3D printing techniques.

Classification	Principle	Variety of Methods	Advantage	Disadvantage
Powder bed fusion	Energy is focused on melting a layer of powder on a bed.	Fused by Heat, Laser, or Electron beams	Applicable to a wide range of metals, ceramics, and polymers	Energy- and time-consuming
Direct energy deposition	Energy is focused on melting materials during their deposition.	Laser engineering net shape (LENS), Electron beam additive manufacturing (EBAM), Wire arc additive manufacturing (WAAM)	Achieves large 3D objects with good mechanical properties in a relatively short time	Relatively expensive
Sheet lamination	2D sheets are stacked and laminated.	Laminated by Ultrasonic welding, Brazing, or Diffusion bonding	Cost-effective for producing large 3D objects	Anisotropy and distortion susceptibility of products
Binder jetting	Powders are bound by a selectively deposited binder adhesive.	Jetting using Phenolic, Silicate, or Aqueous-based binders	Applicable to a wide range of metals, ceramics, and polymers	Inferior mechanical properties due to binders
Material jetting	Droplets of materials are deposited and cured by heat or light.	PolyJet, Nanoparticle jetting, Drop-on demand	Achieving smooth surface and delicate features with high resolution	Not applicable to a wide range of materials
Vat photopolymerization	Photopolymers are selectively cured by exposure to UV or visible light.	Stereolithography, Direct light processing, Continuous liquid interface production	Achieves smooth surface and delicate features with high resolution	Limited choices and properties of photopolymers
Extrusion	Materials are extruded through a nozzle for layer-by-layer deposition.	Extrusion free-forming, and Fused filament fabrication	Cost-effective for producing polymer composites	Low resolution and hence, unsuitable for delicate features

**Figure 2.** Examples of additive manufacturing processes for magnetic materials: (a) selective laser melting; (b) extrusion.

The enhancement of maximum energy product is vital to the prospect of 3D-printed permanent magnets. The magnetic particle alignment by an external magnetic field during extrusion was demonstrated by Sonnleitner et al., as a route to raise the maximum energy product [20]. The in situ magnetic field has been used extensively in the extrusion of rare-earth magnets. Khazdozian et al., showed that the magnetic field of 2.5 kOe was sufficient to align Nd-Fe-B powders in nylon during the extrusion of anisotropic-bonded magnets [21]. With magnetic fields of 0.15 kOe applied in the fused filament fabrication, magnetic alignment in printed samarium cobalt and Nd-Fe-B-based magnets increased the maximum energy product [22]. The particle trajectory and distribution during extrusion through a 3D printer nozzle were modeled by Sarkar et al. [23].

### 3. 3D Printing of Rare-Earth-Free Permanent Magnetic Alloys

Alnico was a widely-used permanent magnet before the market became dominated by rare-earth magnets. Alnico magnets are conventionally produced by either directional solidified casting or powder metallurgy. The classification into alnico 1 through 9 is based on varying iron, aluminium, nickel, cobalt, copper, and titanium compositions. They possess high remanence but moderate coercivity, giving rise to the maximum energy product of up to 10.5 MGOe. The coercivity can be enhanced with increasing shape anisotropy after annealing in a magnetic field. Their thermal stability is advantageous in operations at temperatures as high as 200 °C. White et al., fabricated net-shape alnico

magnets with arbitrary designs and varying alloy compositions by laser engineered net shaping (LENS) of 70–200 W [24,25] and electron beam melting up to 1300 °C [25]. These direct energy deposition and powder-bed fusion approaches using gas atomized powders gave rise to good mechanical properties and the possibility of reducing cobalt content used in commercial alnico 8 and alnico 9. The 3D-printed magnets exhibited remanence as high as 9 kG and the maximum coercivity of 2 kOe, comparable to cast and sintered magnets with comparable compositions. Rottmann et al., also prepared alnico by selective laser melting of 170 W and reported similar microstructures to those obtained by conventional casting and powder metallurgy [26]. Furthermore, the laser was also used in additive manufacturing of  $\text{AlCo}_x\text{Cr}_{1-x}\text{FeNi}$  alloys ( $0 \leq x \leq 1$ ), whose magnetic properties were largely varied with  $x$  [27].

Among manganese-based alloys, the 3D printing development has been focused on MnAl. Radulov et al., used electron beam melting to fabricate MnAl-based permanent magnets [28]. The powder-bed fusion utilized an electron beam with a maximum current of 30 mA to produce fully dense magnets from ball-milled powders without any binder. In a chamber with an average temperature of 830 °C, 3D magnets were formed layer-by-layer with a thickness of 100  $\mu\text{m}$ . The subsequent annealing treatment was needed to promote the ferromagnetic  $\tau$ -MnAl phase from 8% to 90%. The coercivity of the magnet from this electron beam melting was 1.5 kOe, comparable to those from the conventional melting process. Magnetic and mechanical properties were superior, but such a high-cost system was not widely available. Alternatively, fuse filament fabrication has been implemented as an additive manufacturing technique without the high-temperature melting of materials. To this end, thermoplastic composites with high magnetic particle loadings are first produced. Magnetic polymer composites are sensitive to the properties and loading of magnetic powders, as well as their distribution within the polymeric matrix. They were usually drawn into filaments for extrusion. The 3D printers customized for fuse filament fabrication are commercially available at a much lower cost than laser and electron beam sources. Their resolution limit of printing may be acceptable for permanent magnets without demands of high accuracy and delicate features. Palmero et al., prepared MnAl particles with the addition of carbon (MnAl(C)) to stabilize the ferromagnetic  $\tau$  phase [29]. Magnetic powders up to 72.3% were loaded into a polyethylene (PE) matrix via solution casting. Composite filaments are homogeneous and exhibit a coercivity of around 1.5 kOe, matching that obtained from electron beam melting. Their magnetization is proportional to the magnetic loading in the composites. Palmero et al., also fabricated permanent magnetic filaments by loading approximately 80 wt.% MnAl(C) in acryl butadiene styrene (ABS) [30]. Using coarse magnetic powders enhanced the composites' magnetization, whereas finer particles resulted in a higher coercivity. Interestingly, the magnetization normalized with the loading factor of both MnAl(C)-PE and MnAl(C)-ABS being not degraded by the composite synthesis and filament extrusion. Magnetic properties of filaments with the highest loading from each work are compared in Table 2.

**Table 2.** Properties of magnetic filaments for fused filament fabrication.

Magnetic Materials	Polymer Matrix	Magnetic Loading (wt.%)	Extrusion Temperature (°C)	Coercivity (kOe)	Remanent Magnetization (emu/g)	Maximum Magnetization (emu/g)	Reference
MnAl(C)	PE	72	120	1.5	26	58	[29]
MnAl(C)	ABS	80	150	1.8	29	52	[30]
BaFe <sub>12</sub> O <sub>19</sub>	ABS	67	210	1.3	N/A	N/A	[31]
SrFe <sub>12</sub> O <sub>19</sub>	EEA	92	70	3.0	35	62	[32]

In addition to manganese-based alloys, iron nitride ( $\text{Fe}_{16}\text{N}_2$ ) has been developed as a rare-earth-free magnetic material thanks to its large saturation magnetization [33]. Zirhli et al., synthesized  $\text{Fe}_{16}\text{N}_2$  by reducing and then nitriding Fe flakes obtained from surfactant-assisted high-energy ball milling [34]. The  $\text{Fe}_{16}\text{N}_2$  flakes were incorporated into photoresist SU8. The obtained magnetic paste was then extruded by a 3D printer. Extrusion systems

for magnetic filaments and composites in other forms, available in varying scales, provide viable options for a large production volume.

#### 4. 3D Printing of Rare-Earth-Free Permanent Magnetic Ceramics

Strontium hexaferrite ( $\text{SrFe}_{12}\text{O}_{19}$ ) and barium hexaferrite ( $\text{BaFe}_{12}\text{O}_{19}$ ) are prominent ferrimagnetic ceramics. Their commercial applications can be enhanced by developing appropriate 3D printing procedures. The fuse filament fabrication process can be used, similar to MnAl-based magnets, with extrusion temperatures of 70–300 °C. Ferrite powders were firstly incorporated into a thermoplastic matrix, and the obtained composites were then drawn into filaments. Magnetic structures with different geometries could then be produced from extruded filaments. Hanemann et al., produced  $\text{BaFe}_{12}\text{O}_{19}$ -ABS with magnetic loadings up to 76 wt.% [31]. With increasing magnetic loading, the maximum energy product was increased, but mechanical properties deteriorated. The rheological properties were also studied to find appropriate conditions for filament drawing and 3D printing. Palmero et al., used  $\text{SrFe}_{12}\text{O}_{19}$  particles with even higher loadings over 90 wt.% in ethylene ethyl acrylate (EEA) [32]. Extruded composite strips and filaments exhibited homogeneous morphology without deteriorating the magnetic properties of  $\text{SrFe}_{12}\text{O}_{19}$  particles. Table 2 also compared the magnetic properties of ferrite filaments. Interestingly, Sonnleitner et al., improved the magnetic properties by applying an external magnetic field to magnetic particles in the fuse filament fabrication [20]. The alignment of  $\text{SrFe}_{12}\text{O}_{19}$  particles in the polyamides by a 2 kOe magnetic field enhanced the remanence of 3D-printed anisotropic magnets over that of pressed powders.

Vat photopolymerization is an additive manufacturing process by curing a pre-polymer into a solid structure under light exposure. The system has a higher cost but achieves a higher printing resolution than fuse filament fabrication. Nagarajan et al., found that the thickness setting and print region affected the magnets from a commercial 3D printer with a resolution of 50  $\mu\text{m}$  on the X- and Y-axes and 10–100  $\mu\text{m}$  on the Z-axis [35]. Moreover,  $\text{SrFe}_{12}\text{O}_{19}$  particles between stacked layers were aggregated by magnetic attraction. The depth of light penetration and the critical energy of polymerization were studied from curing material using ultraviolet light with varying energies. The printing of magnetic suspensions with  $\text{SrFe}_{12}\text{O}_{19}$  loadings of 10 wt.% and 25 wt.% led to some defects [36]. Both tensile and magnetic properties of strontium ferrite composites were inferior to those of Nd-Fe-B-based composites with the same magnetic loading. Nagarajan et al., also tested in situ polymerization and jetting-based additive manufacturing [37]. Magnetic pastes were prepared by loading 80 wt.%  $\text{SrFe}_{12}\text{O}_{19}$  particles in epoxy resin and a bulk magnet was then obtained from a jetting process. This important work demonstrates that jetting is applicable to hard magnetic materials, and highly dense magnets with delicate features may be obtained from this technique in the future. However, the coercivity and magnetization from the jetting in this work are lower than those of extruded ferrites in Table 3.

**Table 3.** Magnetic properties of 3D-printed hard ferrites.

Magnetic Materials	Fabrication Methods	Printing Speed (mm/s)	Maximum Magnetization (emu/g)	Remanence (kG)	Coercivity (kOe)	Maximum Energy Product (MGOe)	Reference
$\text{SrFe}_{12}\text{O}_{19}$	Jetting	N/A	54	N/A	1.8	N/A	[37]
$\text{SrFe}_{12}\text{O}_{19}$	Extrusion	N/A	N/A	2.2	3.5	N/A	[20]
$\text{SrFe}_{12}\text{O}_{19}$	Extrusion	20	N/A	3.8	3.4	3.31	[38]
$\text{SrFe}_{12}\text{O}_{19}$	Extrusion	5	70	N/A	5.0	2.51	[39]
$\text{BaFe}_{12}\text{O}_{19}$	Extrusion	5	66	N/A	4.0	2.24	[39]
$\text{BaFe}_{12}\text{O}_{19}$	Extrusion	5	65	N/A	2.3	N/A	[40]

Extrusion free-forming is a promising route for printing bulk ferrites with diverse geometries. Like other extrusion varieties, a large fabrication volume is attainable at

a relatively low cost. Peng et al., successfully fabricated  $\text{BaFe}_{12}\text{O}_{19}$  from  $\text{BaCO}_3$  and  $\text{Fe}_2\text{O}_3$  precursors, and the ceramic paste was extruded through a nozzle of commercial 3D printers [40]. After sintering at 1200–1400 °C, dense  $\text{BaFe}_{12}\text{O}_{19}$  magnets were obtained with minimal porosity. The magnetization as high as 95% of the  $\text{BaFe}_{12}\text{O}_{19}$  theoretical bulk magnetization values was achieved in the case of 1200 °C. Wei et al., prepared net-shaped  $\text{BaFe}_{12}\text{O}_{19}$  and  $\text{SrFe}_{12}\text{O}_{19}$  magnets by the extrusion free-forming process [39]. Their saturation magnetizations were close to the theoretical values, and the coercivities were enhanced over those obtained from the conventional ceramic processing to 4–6 kOe. The maximum energy product was as high as 2.5 MGOe in the case of 3D-printed  $\text{SrFe}_{12}\text{O}_{19}$  magnets. Magnetic properties were markedly varied with the sintering temperature from 950 °C to 1250 °C. The grain growth by the sintering at 1250 °C substantially decreased the maximum energy product because of the coercivity decrease in multidomain ferrites. The highest value of the maximum energy product was obtained in the magnets sintered at 1150 °C, listed along with other parameters in Table 2. Yang et al., fabricated complex-shaped  $\text{SrFe}_{12}\text{O}_{19}$  magnets from 3D gel-printing [38]. The hydroxyethyl methacrylate gelation system contained strontium hexaferrite powders with 1 wt.% silane as a coupling agent and 2.5 vol.% polymer Silok7050S as a dispersant. The pseudo-plastic slurries were extruded to form magnets. The subsequent sintering at 1300 °C resulted in the maximum magnetic energy product of 3.31 MGOe, the highest value in Table 3. Yang et al., also mixed  $\text{SrFe}_{12}\text{O}_{19}$  with  $\text{NdFeB}$  to increase the maximum energy product of 3D-printed magnets [41].

## 5. Computer Simulations and Applications of 3D-Printed Rare-Earth-Free Magnets

Magnetic materials produced by 3D printing technology have primary applications in electrical machines [42]. Motors, generators, and flywheel energy storage systems utilize hard and soft magnetic components with varying shapes and dimensions [43]. Recent developments in soft magnetic mesh, gears, rings, and cylinders for electrical machines are reviewed [44]. On the other hand, hard magnets directly influence the efficiency and performance of electrical machines [45]. For example, the motor efficiency is enhanced with increasing magnetic flux distribution, and its performance is degraded by demagnetization at elevated temperatures [46]. Applications of printable magnetic structures are also in sensing and energy harvesting [47].

The developments in materials and device integrations are facilitated by advancements in the computation of magnetic materials and fields. Magpylib, an open-source Python package, can simulate magnetic fields from different sets of permanent magnets of varying geometries [48]. A user-friendly scripting interface allows access to a library of analytical solutions for the magnetic field. Source objects are magnets generating a magnetic field in a 3D Euclidean space. The dimension, position, and orientation of the source magnet can then be used for geometric manipulation and magnetic field calculation. To optimize the design of permanent magnets, Kovacs et al., used multiscale simulations with a sequence ranging from the atomic scale to determine the achievable performance in rare-earth-free magnetic materials [49]. The micromagnetic simulation used intrinsic parameter input for predicting extrinsic magnetic properties of materials with geometric variations. The effect of the grain boundary phase was analyzed by a Python script controlling the open-source computer-aided design (CAD) software Salome. The structure of MnAl magnets was optimized by a machine learning algorithm, resulting in the coercivity and maximum energy product of 5.3 kOe and 10 MGOe, respectively. The computation for a higher coercivity, using the open-source optimization framework Dakota, revealed values of less than 10 kOe in most rare-earth-free magnets.

Furthermore, Kontos and colleagues simulated the integration of rare-earth-free MnAl magnets in electrical machines using COMSOL Multiphysics 5.4 software [50]. Assuming ideal conditions, a hysteresis loop was calculated using measured and computed saturation magnetization values. They utilized experimental MnAl data on generators with different permanent magnets for simulations. As input parameters, the value and

direction of remanent magnetization were investigated. However, important factors such as thermal properties, mechanical stability, and demagnetization should be included in these simulations before verifying with an experiment. The optimizations of permanent magnetic coupling to minimize the coupling volume and maximize the magnetic torque have predominantly been carried out on rare-earth Nd-Fe-B magnets [51]. The optimization incorporated Matlab, SolidWorks, and Simcenter MagNet software programs, within Visual Studio. The designs were compared in terms of volume, magnetic torque, and magnetic torque density. The permanent magnetic couplings using the genetic algorithm and Taguchi optimization method are identical, but the latter is considerably more time-efficient.

## 6. Conclusions

The advantages of additive manufacturing technology over conventional processes have been demonstrated in producing rare-earth-free magnetic alloys and ceramics with varying shapes and dimensions. The use of rare-earth-free materials also increases supply stability. Laser and electron beam melting successfully produced alnico magnets. Electron beam melting was also used with MnAl alloys, and stereolithography was demonstrated on strontium ferrites. Both strontium ferrite and MnAl magnets can be printed using fuse filament fabrication with high magnetic loadings in thermoplastics. The extrusions of hard ferrites were also accomplished from magnetic pastes. Interestingly, the magnetic properties of 3D-printed alloys from selective laser melting and hard ferrites from fuse filament fabrication were comparable to those of conventional sintered and bonded magnets with the same compositions. Furthermore, the magnetic properties may be enhanced by aligning magnetic particles with an external magnetic field during the extrusion of magnetic pastes or filaments. Whereas their performances were inferior to the rare-earth counterparts, these rare-earth-free magnets can still be essential parts of efficient electrical machines and smart structures. Software packages are available for designing magnets and optimizing their performance in a simulation before their implementation. By taking advantage of magnetically active components, the potential of many smart structures and systems can be fulfilled.

**Author Contributions:** Conceptualization, C.S.; methodology, C.S. and Y.S.; validation, C.S. and Y.S.; formal analysis, C.S.; investigation, C.S.; resources, C.S. and Y.S.; data curation, C.S.; writing—original draft preparation, C.S. and Y.S.; writing—review and editing, C.S. and Y.S.; project administration, C.S.; funding acquisition, C.S. All authors have read and agreed to the published version of the manuscript.

**Funding:** This research was funded by the Thailand Excellent Center in Physics, grant number ThEP-63-PIP-WU3.

**Data Availability Statement:** Not applicable.

**Acknowledgments:** Figures are drawn by Wannisa Thongsamrit.

**Conflicts of Interest:** The authors declare no conflict of interest.

## References

1. Hirose, S.; Nishino, M.; Miyashita, S. Perspectives for high performance permanent magnets: Applications, coercivity, and new materials. *Adv. Nat. Sci. Nanosci. Nanotechnol.* **2017**, *8*, 013002. [[CrossRef](#)]
2. Coey, J.M.D. Perspective and prospects for rare earth permanent magnets. *Engineering* **2020**, *6*, 119–131. [[CrossRef](#)]
3. Pullar, R.C. Hexagonal ferrites: A review of the synthesis, properties and applications of hexaferrite ceramics. *Prog. Mater. Sci.* **2012**, *57*, 1191–1334. [[CrossRef](#)]
4. Yan, D.; Ro, S.O.S.; Kim, S. On the global rare earth elements utilization and its supply-demand in the future. *IOP Conf. Ser. Earth Environ. Sci.* **2020**, *508*, 012084. [[CrossRef](#)]
5. Li, D.; Pan, D.S.; Li, S.J.; Zhang, Z.D. Recent developments of rare-earth-free hard-magnetic materials. *Sci. China Phys. Mech. Astron.* **2016**, *59*, 617501. [[CrossRef](#)]
6. Cui, J.; Kramer, M.; Zhou, L.; Liu, F.; Gabay, A.; Hadjipanayis, G.; Balasubramanian, B.; Sellmyer, D. Current progress and future challenges in rare-earth-free permanent magnets. *Acta Mater.* **2018**, *158*, 118–137. [[CrossRef](#)]
7. Yang, J.; Yang, W.; Shao, Z.; Liang, D.; Zhao, H.; Xia, Y.; Yang, Y. Mn-based permanent magnets. *Chin. Phys. B* **2018**, *27*, 117503. [[CrossRef](#)]

8. Marenkina, S.F.; Ril'a, A.I. Al–Mn hard magnetic alloys as promising materials for permanent magnets (Review). *Russ. J. Inorg. Chem.* **2020**, *65*, 2007–2019. [[CrossRef](#)]
9. Sarkar, A.; Mallick, A.B. Synthesizing the hard magnetic low-temperature phase of MnBi alloy: Challenges and prospects. *JOM* **2020**, *72*, 2812–2825. [[CrossRef](#)]
10. Sirisathitkul, C. Recent developments of manganese-aluminium as rare-earth-free magnets. *Adv. Mat. Res.* **2020**, *9*, 323–335. [[CrossRef](#)]
11. Poudyal, N.; Liu, J.P. Advances in nanostructured permanent magnets research. *J. Phys. D Appl. Phys.* **2013**, *46*, 043001. [[CrossRef](#)]
12. Additive Manufacturing. Available online: <https://engineeringproductdesign.com/knowledge-base/additive-manufacturing-processes/> (accessed on 10 August 2022).
13. Li, L.; Post, B.; Kunc, V.; Elliott, A.M.; Paranthaman, M.P. Additive manufacturing of near-net-shape bonded magnets: Prospects and challenges. *Scr. Mater.* **2017**, *135*, 100–104. [[CrossRef](#)]
14. Popov, V.; Koptyug, A.; Radulov, I.; Maccari, F.; Muller, G. Prospects of additive manufacturing of rare-earth and non-rare-earth permanent magnets. *Procedia Manuf.* **2018**, *21*, 100–108. [[CrossRef](#)]
15. Périgo, E.A.; Jacimovic, J.; Ferré, F.G.; Scherf, L.M. Additive manufacturing of magnetic materials. *Addit. Manuf.* **2019**, *30*, 100870. [[CrossRef](#)]
16. Chaudhary, V.; Mantri, S.A.; Ramanujan, R.V.; Banerjee, R. Additive manufacturing of magnetic materials. *Prog. Mater. Sci.* **2020**, *114*, 100688. [[CrossRef](#)]
17. Goll, D.; Schurr, J.; Trauter, F.; Schanz, J.; Bernthaler, T.; Riegel, H.; Schneider, G. Additive manufacturing of soft and hard magnetic materials. *Procedia CIRP* **2020**, *94*, 248–253. [[CrossRef](#)]
18. Charoensuk, T. Complex near-net-shape bonded magnet fabrication by additive manufacturing. *Thai J. Phys.* **2021**, *38*, 39–53.
19. Silva, T.F.V.; Stoppa, M.H. Production of complex shape magnets using additive manufacturing: A state-of-the-art analysis. *J. Thermoplast. Compos. Mater.* **2022**, *35*, 1041–1058. [[CrossRef](#)]
20. Sonnleitner, K.; Huber, C.; Teliban, I.; Kobe, S.; Saje, B.; Kagerbauer, D.; Reissner, M.; Lengauer, C.; Groenefeld, M.; Suess, D. 3D printing of polymer-bonded anisotropic magnets in an external magnetic field and by a modified production process. *Appl. Phys. Lett.* **2020**, *116*, 092403. [[CrossRef](#)]
21. Khazdozian, H.A.; Li, L.; Paranthaman, M.P.; McCall, S.K.; Kramer, M.J.; Nlebedim, I.C. Low-field alignment of anisotropic bonded magnets for additive manufacturing of permanent magnet motors. *JOM* **2019**, *71*, 626–632. [[CrossRef](#)]
22. Sarkar, A.; Somashekara, M.A.; Paranthaman, M.P.; Kramer, M.; Haase, C.; Nlebedim, I.C. Functionalizing magnet additive manufacturing with in-situ magnetic field source. *Addit. Manuf.* **2020**, *34*, 101289. [[CrossRef](#)]
23. Sarkar, A.; Paranthaman, M.P.; Nlebedim, I.C. In-situ magnetic alignment model for additive manufacturing of anisotropic bonded magnets. *Addit. Manuf.* **2021**, *46*, 102096. [[CrossRef](#)]
24. White, E.M.H.; Kassen, A.G.; Simsek, E.; Tang, W.; Ott, T.T.; Anderson, I.E. Net shape processing of alnico magnets by additive manufacturing. *IEEE Trans. Magn.* **2017**, *53*, 2101606. [[CrossRef](#)]
25. White, E.; Rinko, E.; Prost, T.; Horn, T.; Ledford, C.; Rock, C.; Anderson, I. Processing of alnico magnets by additive manufacturing. *Appl. Sci.* **2019**, *9*, 4843. [[CrossRef](#)]
26. Rottmann, P.F.; Polonsky, A.T.; Francis, T.; Emigh, M.G.; Krispin, M.; Rieger, G.; Echlin, M.P.; Levi, C.G.; Pollock, T.M. TriBeam tomography and microstructure evolution in additively manufactured alnico magnets. *Mater. Today* **2021**, *49*, 23–34. [[CrossRef](#)]
27. Borkar, T.; Chaudhary, V.; Gwalani, B.; Choudhuri, D.; Mikler, C.V.; Soni, V.; Alam, T.; Ramanujan, R.V.; Banerjee, R. A combinatorial approach for assessing the magnetic properties of high entropy alloys: Role of Cr in AlCo<sub>x</sub>Cr<sub>1-x</sub>FeNi. *Adv. Eng. Mater.* **2017**, *19*, 1700048. [[CrossRef](#)]
28. Radulov, I.A.; Popov, V.V., Jr.; Koptyug, A.; Maccari, F.; Kovalevsky, A.; Essel, S.; Gassmann, J.; Skokov, K.P.; Bamberger, M. Production of net-shape Mn–Al permanent magnets by electron beam melting. *Addit. Manuf.* **2019**, *30*, 100787. [[CrossRef](#)]
29. Palmero, E.M.; Rial, J.; de Vicente, J.; Camarero, J.; Skårman, B.; Vidarsson, H.; Larsson, P.O.; Bollero, A. Development of permanent magnet MnAlC/polymer composites and flexible filament for bonding and 3D-printing technologies. *Sci. Technol. Adv. Mater.* **2018**, *19*, 465–473. [[CrossRef](#)]
30. Palmero, E.M.; Casaleiz, D.; de Vicente, J.; Skårman, B.; Vidarsson, H.; Larsson, P.O.; Bollero, A. Effect of particle size distribution on obtaining novel MnAlC-based permanent magnet composites and flexible filaments for 3D-printing. *Addit. Manuf.* **2020**, *33*, 101179. [[CrossRef](#)]
31. Hanemann, T.; Syperek, D.; Nötzel, D. 3D printing of ABS barium ferrite composites. *Materials* **2020**, *13*, 1481. [[CrossRef](#)]
32. Palmero, E.M.; Casaleiz, D.; Jiménez, N.A.; Rial, J.; de Vicente, J.; Nieto, A.; Altimira, R.; Bollero, A. Magnetic-polymer composites for bonding and 3D printing of permanent magnets. *IEEE Trans. Magn.* **2019**, *55*, 2101004. [[CrossRef](#)]
33. Li, D.; Li, Y.; Pan, D.; Zhang, Z.; Choi, C.J. Prospect and status of iron-based rare-earth-free permanent magnetic materials. *J. Magn. Magn. Mater.* **2019**, *469*, 535–544. [[CrossRef](#)]
34. Zirhli, O.; Akdogan, N.G.; Odeh, Y.N.; Misirlioglu, I.B.; Devlin, E.; Akdogan, O. Fabrication and characterization of Fe<sub>16</sub>N<sub>2</sub> micro-flake powders and their extrusion based 3D printing into permanent magnet form. *Adv. Eng. Mater.* **2020**, *22*, 2000311. [[CrossRef](#)]
35. Nagarajan, B.; Arshad, M.; Ullah, A.; Mertiny, P.; Qureshi, A.J. Additive manufacturing ferromagnetic polymers using stereolithography: Materials and process development. *Manuf. Lett.* **2019**, *21*, 12–16. [[CrossRef](#)]



36. Nagarajan, B.; Mertiny, P.; Qureshi, A.J. Magnetically loaded polymer composites using stereolithography: Material processing and characterization. *Mater. Today Commun.* **2020**, *25*, 101520. [[CrossRef](#)]
37. Nagarajan, B.; Kamkar, M.; Schoen, M.A.W.; Sundararaj, U.; Trudel, S.; Qureshi, A.J.; Mertiny, P. Development and characterization of stable polymer formulations for manufacturing magnetic composites. *J. Manuf. Mater. Process.* **2020**, *4*, 4. [[CrossRef](#)]
38. Yang, F.; Zhang, X.; Guo, Z.; Volinsky, A.A. 3D gel printing of Sr ferrite parts. *Ceram. Int.* **2018**, *44*, 22370–22377. [[CrossRef](#)]
39. Wei, X.; Liu, Y.; Zhao, D.; Mao, X.; Jiang, W.; Ge, S.S. Net-shaped barium and strontium ferrites by 3D printing with enhanced magnetic performance from milled powders. *J. Magn. Magn. Mater.* **2020**, *493*, 165664. [[CrossRef](#)]
40. Peng, E.; Wei, X.; Herng, T.S.; Garbe, U.; Yub, D.; Ding, J. Ferrite-based soft and hard magnetic structures by extrusion free-forming. *RSC Adv.* **2017**, *7*, 27128–27138. [[CrossRef](#)]
41. Yang, F.; Zhang, X.; Guo, Z.; Ye, S.; Sui, Y.; Volinsky, A.A. 3D printing of NdFeB bonded magnets with SrFe<sub>12</sub>O<sub>19</sub> addition. *J. Alloys Compd.* **2019**, *779*, 900–907. [[CrossRef](#)]
42. Zhang, C.; Li, X.; Jiang, L.; Tang, D.; Xu, H.; Zhao, P.; Fu, J.; Zhou, Q.; Chen, Y. 3D printing of functional magnetic materials: From design to applications. *Adv. Funct. Mater.* **2021**, *31*, 2102777. [[CrossRef](#)]
43. Bernier, F.; Ibrahim, M.; Mihai, M.; Thomas, Y.; Lamarre, J.M. Additive manufacturing of soft and hard magnetic materials used in electrical machines. *Met. Powder Rep.* **2020**, *75*, 334–3431. [[CrossRef](#)]
44. Lamichhane, T.N.; Sethuraman, L.; Dalagan, A.; Wang, H.; Keller, J.; Paranthaman, M.P. Additive manufacturing of soft magnets for electrical machines: A review. *Mater. Today Phys.* **2020**, *15*, 100255. [[CrossRef](#)]
45. Naseer, M.U.; Kallaste, A.; Asad, B.; Vaimann, T.; Rassölkin, A. A review on additive manufacturing possibilities for electrical machines. *Energies* **2021**, *14*, 1940. [[CrossRef](#)]
46. Gundabattini, E.; Kuppan, R.; Solomon, D.G.; Kalam, A.; Kothari, D.P.; Abu Bakar, R. A review on methods of finding losses and cooling methods to increase efficiency of electric machines. *Ain Shams Eng. J.* **2021**, *12*, 497–505. [[CrossRef](#)]
47. Wang, Z.; Huber, C.; Hu, J.; He, J.; Suess, D.; Wang, S.X. An electrodynamic energy harvester with a 3D printed magnet and optimized topology. *Appl. Phys. Lett.* **2019**, *114*, 013902. [[CrossRef](#)]
48. Ortner, M.; Bandeira, L.G.C. Magpylib: A free Python package for magnetic field computation. *SoftwareX* **2020**, *11*, 100466. [[CrossRef](#)]
49. Kovacs, A.; Fischbacher, J.; Gusenbauer, M.; Oezelt, H.; Herper, H.C.; Vekilova, O.Y.; Nieves, P.; Arapan, S.; Schrefl, T. Computational design of rare-earth reduced permanent magnets. *Engineering* **2020**, *6*, 148–153. [[CrossRef](#)]
50. Kontos, S.; Ibrayeva, A.; Leijon, J.; Mörée, G.; Frost, A.E.; Schönström, L.; Gunnarsson, K.; Svedlindh, P.; Leijon, M.; Eriksson, S. An overview of MnAl permanent magnets with a study on their potential in electrical machines. *Energies* **2020**, *13*, 5549. [[CrossRef](#)]
51. Andriushchenko, E.; Kallaste, A.; Belahcen, A.; Vaimann, T.; Rassölkin, A.; Heidari, H.; Tiismus, H. Optimization of a 3D-printed permanent magnet coupling using genetic algorithm and Taguchi method. *Electronics* **2021**, *10*, 494. [[CrossRef](#)]